

## Article

# Comparison of Impervious Surface Dynamics through Vegetation/High-Albedo/Low-Albedo/Soil Model and Socio-Economic Factors

Kapo Wong <sup>1</sup> , Yuanzhi Zhang <sup>2,3,\*</sup>, Qiuming Cheng <sup>4</sup>, Ming Chun Chao <sup>5</sup> and Jin Yeu Tsou <sup>5</sup> 

<sup>1</sup> School of Nursing, The Hong Kong Polytechnic University, Hong Kong 999666, China; portia.wong@polyu.edu.hk

<sup>2</sup> School of Marine Science, Nanjing University of Information Science and Technology, Nanjing 210044, China

<sup>3</sup> Center for Housing Innovations, Institute of Asia-Pacific Studies, Faculty of Social Science, Chinese University of Hong Kong, Hong Kong 999777, China

<sup>4</sup> School of Earth Sciences and Engineering, Sun Yat-sen University, Zhuhai 519000, China; qiuming.cheng@iugs.org

<sup>5</sup> Department of Architecture and Civil Engineering, City University of Hong Kong, Hong Kong 999666, China; mcchao@cityu.edu.hk (M.C.C.); jytsou@cityu.edu.hk (J.Y.T.)

\* Correspondence: yzhang209@nuist.edu.cn or yuanzhizhang@cuhk.edu.hk; Tel.: +86-188-8885-3470

**Abstract:** Hong Kong and Shenzhen have entirely different land-use development policies, resulting in a disparity in the increase rate of impervious surface area. Impervious surface estimation is a significant method for evaluating urbanization, so that countries and cities can deal with their growing populations. The impervious surface area was estimated through Landsat Thematic Mapper (TM) image extraction, the V-H-L-S (vegetation, high-albedo, low-albedo, and soil) model, and linear spectral un-mixing analysis (LSUM). Changes in fractions of endmembers over periods of time were identified and employed to analyze changes in land use and land cover (LULC). The research adopting the V-H-L-S model for classifying land cover and exploring the association of change in impervious surface areas and socio-economic growth over a period of time is limited. In this study, impervious surface estimations for Hong Kong and Shenzhen in 1995, 2005, and 2016 were compared, selecting vegetation, high-albedo, low-albedo, and soil as endmembers. The change rate of the fractions in the four endmembers was calculated to identify changes in land use and land cover during these three specific time periods. The impervious surface was determined to constitute a combination of high-albedo and low-albedo. Moreover, a proportional relationship exists between the increase in impervious surface area, population rate, GDP, and GDP per capita in both Hong Kong and Shenzhen. However, there was a difference in the increase in impervious surface area between Hong Kong and Shenzhen due to the different land-use policies in the country's two systems.

**Keywords:** impervious surface; V-H-L-S model; linear spectrum un-mixing analysis; endmember; urbanization



**Citation:** Wong, K.; Zhang, Y.; Cheng, Q.; Chao, M.C.; Tsou, J.Y. Comparison of Impervious Surface Dynamics through Vegetation/High-Albedo/Low-Albedo/Soil Model and Socio-Economic Factors. *Land* **2022**, *11*, 430. <https://doi.org/10.3390/land11030430>

Academic Editors: David Pastor-Escuredo, Alfredo J. Morales and Yolanda Torres

Received: 14 February 2022

Accepted: 10 March 2022

Published: 16 March 2022

**Publisher's Note:** MDPI stays neutral with regard to jurisdictional claims in published maps and institutional affiliations.



**Copyright:** © 2022 by the authors. Licensee MDPI, Basel, Switzerland. This article is an open access article distributed under the terms and conditions of the Creative Commons Attribution (CC BY) license (<https://creativecommons.org/licenses/by/4.0/>).

## 1. Introduction

Land-use policy has had a significant influence on urban development, as well as the spatial distribution of impervious surfaces within countries, which has been a major factor in controlling the rate and pattern of urbanization [1,2]. There are impervious surfaces [3], a significant element in evidencing urbanization [4], in a variety of countries, and there are cases in which water cannot penetrate through the outermost surface material to the soil beneath. Asphalt, brick, and concrete are impervious materials used in infrastructure, which can indicate the development of urbanization, resulting in an increase in land for buildings, especially residential, commercial, and industrial, along with roads for connecting the infrastructure.

Remote sensing constitutes a common approach to assess impervious surface changes, and its validity and reliability in conducting impervious surface assessments have been proven by many previous studies using Landsat and other satellites [5,6]. The V-I-S (vegetation-impervious surface-soil) model is a conceptual model for analyzing urban environments [7], which assumes that the surface cover of land is composed of vegetation, impervious surface, and soil, which provides a foundation for analysis of urban geography, biophysical geography, and human systems. For example, impervious surfaces have continued to increase due to rapid urbanization, resulting in a decline in the amount of vegetation. Moreover, human–land interaction drives the change in land use and global processes, such as biodiversity loss and ecosystem degradation. Appropriate management and policies on human–environment interaction could be implemented to prevent any environmental problem or inadvertent impact. The model could also be applied to observe the ratio of land and sea, as water is excluded in the model. The V-I-S model is not a holistic analytical model for urban land use, since it only provides three classifications of land cover. An impervious surface is an endmember, which comprises a wide variety of materials [8], such as asphalt, concrete, and brick, to construct roads, buildings, and infrastructure.

The V-H-L-S model was developed by modifying the V-I-S model [9,10], in which the impervious surface's components were divided into two sub-components, corresponding to more spectral characteristics (i.e., H for high-albedo and L for low-albedo). The V-I-S model is undoubtedly a useful foundation for classifying the urban morphology within and between cities [11]. Combining high-albedo and low-albedo impervious surfaces can cause concern when analyzing the land types for special infrastructure and residential uses. The change in residential land use may be associated with the growth of population in certain areas. However, high-albedo can reflect this feature. For example, in the study of Shih et al. [12], the V-I-S model could not identify the types of urban land uses. The development of the V-H-L-S model is critical in the meticulous classification of urban land uses. Furthermore, the reduction in noise in Landsat images through minimum noise fraction (MNF) transformation, which is a crucial step providing six eigenvalues, aims to enhance the images' significant features. For acceptable eigenvalues with MNF values greater than 1.0, the larger the eigenvalue, the better the spatial features of the selected endmember. Although, as indicated, many previous studies address impervious surface estimation [13,14], no comparison has yet been performed regarding the role of land-use policies in impervious surface dynamic analysis between two systems in one country, such as in Hong Kong and Shenzhen, China.

Hong Kong and Shenzhen are experiencing a dramatic population growth rate due to urbanization. The favorable economic development of the two cities is perhaps the main factor leading to their expanding populations. However, Hong Kong and Shenzhen approach land-use policy in totally different ways. While Shenzhen has experienced a tremendous increase in its urban area, Hong Kong has witnessed a very small increase in the urban area. This phenomenon demonstrates the concept of “one country, two systems,” which has resulted in a remarkable difference in the urban spatial development and the distribution of impervious surfaces between the two cities. This difference also reflects the stark contrast between the land policies in two systems in one country. Socio-economic factors, including population density and unit area gross domestic product, are the significant factors influencing a city's impervious surface areas [15,16]. Therefore, this study sought to: (1) estimate urban impervious surface area and analyze the spatial distribution of Hong Kong and Shenzhen from 1995, 2005, and 2016; (2) explore the association between the impervious surface area change, population, gross domestic product (GDP), and GDP per capita of Hong Kong and Shenzhen from 1995, 2005, and 2016; and (3) compare the change over time of perspectives on urban areas and socio-economic data between Hong Kong and Shenzhen.

## 2. Materials and Methods

### 2.1. Study Area

#### 2.1.1. Hong Kong

Hong Kong is located at the southern end of China, is bounded by the coastline to the east, south, and west (Figure 1), and the total area (land and sea areas) is approximately 2755 km<sup>2</sup>. In 2016, the population was 7.34 million. Rural areas and mountains constitute most of the geography; more than 75% of the land area has not been developed for urban utilization due to its topography. In addition, the city exhibits extremely high density, with more than 7 million people, and the projected population in 2031 is 8 million [17]. Thus, the density problem in Hong Kong is becoming increasingly serious with its limited terrestrial area. Government legislation regarding rural park protection makes it difficult to develop more flat land for urban use. The city also has a high population growth rate, as economic development is strong with the implementation of laissez-faire capitalism [18], positive non-interventionism, its favorable geographic location, and effective information flow. In the 1960s, Hong Kong started to develop light industry, and large numbers of factories were built to fulfill manufacturing demand. However, since inland China implemented the “reform and opening-up” policy, providing a cost incentive to businesses, many businesses relocated to the mainland to establish factories for production. Due to the departure of its manufacturing base, financial and service industries constitute a large percentage of all industries in Hong Kong. Moreover, according to the ranking of city competitiveness in China [19], Hong Kong was ranked number one.

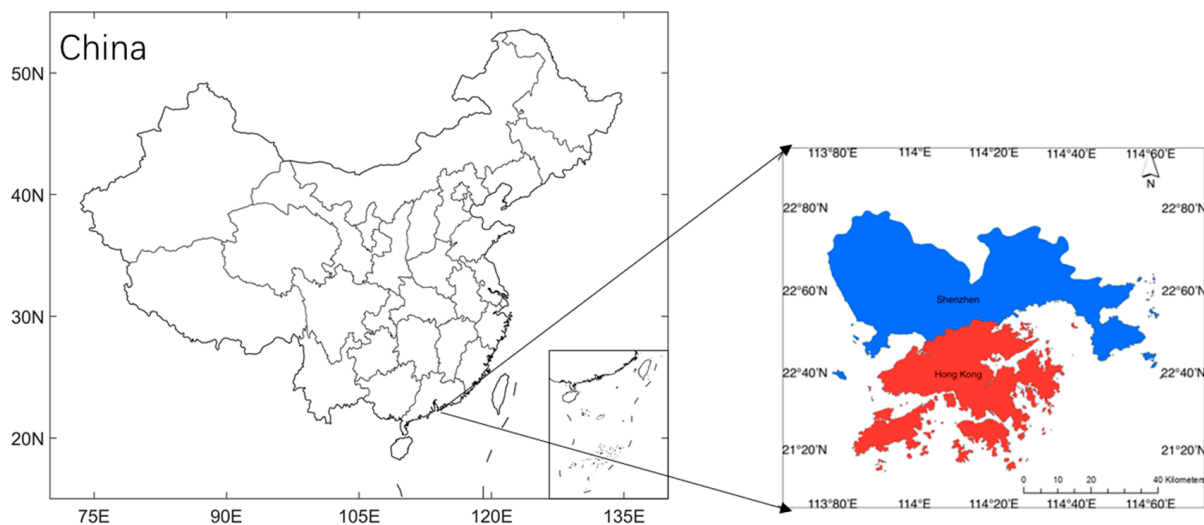


**Figure 1.** Study areas of Hong Kong (red) and Shenzhen (blue).

#### 2.1.2. Shenzhen

Shenzhen is in the southern part of China, adjacent to the northern region of Hong Kong (Figure 1). The total area of Shenzhen is approximately 3140 km<sup>2</sup>, including land and sea areas, with a population of approximately 11.91 million in 2016 [20]. This constitutes a dramatic increase from the 1995 population of 2.39 million, and the projected population in 2030 is approximately 12.67 million. Due to the 2003 cancellation of the policy requiring a permit to purchase a house for permanent residence, the annual population growth rate has been approximately 9–10%. To accommodate this rapid population growth, authorities transformed the hills and rural parks into flatlands and built residential buildings over these areas. The amount of urban area in Shenzhen, therefore, has continued increasing under the official policy. In the 1980s, Shenzhen was developed as the first special economic zone in China with innovative technologies, finance, logistics, and culture as main industries. The aggregate economic volume of Shenzhen ranked second in the Guangdong Province

and fourth in China overall, and the scale of financial assets of Shenzhen was ranked third in China. Network and technology industries, for instance, Alibaba, Baidu, and Tencent, as well as education and research and development have developed rapidly. In addition, the new Shenzhen Bao'an International Airport, in operation since 2013, is the first transportation system to offer comprehensive service in China.

In this study, changes in impervious surface area for Hong Kong and Shenzhen were identified through satellite images and a comparison between the two cities. Regarding data about changes in impervious surface area in Hong Kong and Shenzhen, relationships between the change in urban areas, land-use development policies, population growth, and economic development were analyzed using GDP and per capita GDP data.

## 2.2. Data Sets

The current investigation utilized images from Landsat Thematic Mapper (TM) data for 1995, 2005, and 2016. The dates of a spatial resolution of 30 m  $\times$  30 m Landsat TM images with less cloud cover in 1995, 2005, and 2016 were 2 November, 23 November, and 7 December, respectively (see Table 1). In addition, SPOT and Google Map images, as well as statistical data from Hong Kong and Shenzhen, were employed in data validation and comparison.

**Table 1.** Data information of Landsat TM images.

Year	1995	2005	2016
Date	2 November 1995	23 November 2005	7 December 2016
Sensor Type	Landsat5 TM	Landsat5 TM	Landsat8 OLI

## 2.3. Methodology

Figure 2 shows the procedures of processing the Landsat TM images and extracting impervious surfaces with ENVI software. An atmospheric correction of Landsat images was performed to enhance visibility and increase accuracy for the selection of endmembers. A water mask, which was created for the sea area, water area, and the regions outside of the study areas, was required to cover Landsat images. Subsequently, MNF transform, producing six layers, demonstrated the contribution rate of the dimensionality of each layer [21]. The results of MNF component 1, MNF component 2, and MNF component 3 were applied to the 2D scatter plot to identify the four endmembers, similar as the previous studies [13,14]. As a result, the linear spectral un-mixing analysis was conducted to generate the five fraction's images, corresponding to vegetation, high-albedo, low-albedo, and soil, and root mean square error (RMSE), in which impervious surface was determined by superimposing the images of high-albedo and low-albedo fractions. Albedo is a measure of reflectivity that depends on the amount of light being reflected or absorbed by a surface or material. Shallow objects or surfaces reflect more radiation, resulting in high-albedo, and darker objects absorb more radiation and reflect less light, resulting in low-albedo. The values of high-albedo ranged between 0.4 and 0.7, and the values of low-albedo ranged between 0.04 and 0.4 [22].

In addition, SPOT and Google Earth images were used to validate the fraction's image of impervious surfaces in the selected areas in Hong Kong and Shenzhen [14]. Imagery resolution in SPOT and Google Earth ranges from 6 m to 10 m and from 15 m of resolution to 15 cm, respectively. An urban socio-economic comparison was also performed to elucidate the cause of the change in impervious surface.

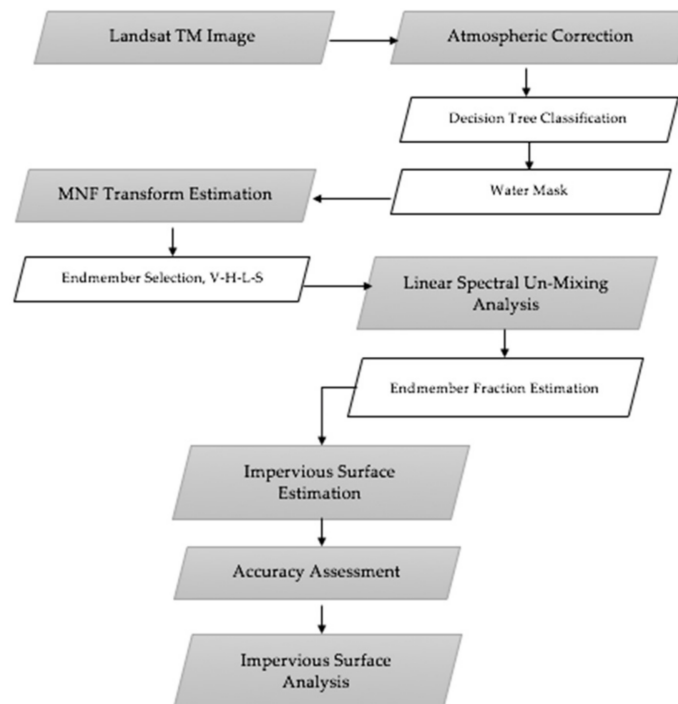


**Figure 2.** Procedure of impervious surface estimation.

### 2.3.1. Linear Spectral Mixture Analysis

Linear spectral mixture analysis (LSMA) is a methodology for resolving pixel mixture problems in impervious surface analysis. A study of LSMA [23] reported that endmembers constitute the composition of surface materials in the land cover in certain pixels. Endmembers that exhibited homogenous spectral on the imagery were considered to be the same type of surface material. Because of its ability to overcome the heterogeneous spectral mixing challenge, a wide variety of land estimations have been performed utilizing the LSMA model, such as vegetation cover, impervious surface, and change detection. Indeed, previous studies extracted impervious surfaces with one endmember or more than one endmember [6,24–26]. The LSMA model was also applied to calculate the fraction of endmembers in a mixed pixel and formula for LSMA:

$$R_i = R \sum_{m=1}^N f_m R_{mi} + e_i \quad (1)$$

$$\sum_{m=1}^N f_m = 1; f_m > 0 \quad (2)$$

$$rms = \sqrt{\frac{1}{n} \sum_{i=1}^n e_i^2} \quad (3)$$

where  $R_i$  is the reflectance of mixed image spectrum at each band  $i$ ;  $f_m$  is the fraction filled by the endmember;  $R_{mi}$  is the reflectance of each endmember at each band;  $e_i$  is the reflectance in band  $b$  without being modeled;  $n$  is the number of image bands; and  $m$  is the number of endmembers.

The estimation of the endmember spectra and the number of endmembers constituted an essential step for analyzing an image in terms of mixtures. The estimation process contained image processing, endmember selection, spectral un-mixing, and evaluating fraction images [14]. In addition, a trial-and-error method was required to obtain the correct number of endmember spectra. Spectral mixing analysis was adopted to resolve the inverse problem to identify fractions of the spectra, which were in proportion to the

amount of endmembers in the pixel. Furthermore, singular value decomposition in ENVI software was employed to handle the least-square problem, in which the number of bands was greater than the number of endmembers. Since endmember selection could affect the result of the LSMA model, at most, four endmembers were identified from the 2D scatter plots after the extraction process of minimum noise fraction [27]. However, the 30 m spatial resolution of the remote sensor data of Thematic Mapper was too coarse for urban study [28]. Medium resolution remote sensor data were utilized in pixel mixing for urban environment analysis [29,30]. To overcome the pixel mixing problem, linear spectral mixture analysis (LSMA) was adopted for extracting information from the data.

### 2.3.2. Accuracy Assessment

The determination coefficient ( $R^2$ ), root mean square error (RMSE), and mean absolute errors (MAE) were employed to discern the accuracy of impervious surface estimation [6]. The equations for RMSE and MAE are as follows:

$$RMSE = \sqrt{\frac{\sum_{i=1}^N (X_i - Y_i)^2}{N}} \quad (4)$$

$$MAE = \frac{1}{N} \sum_{i=1}^N |X_i - Y_i| \quad (5)$$

where  $X_i$  is sample  $i$ 's estimated fraction of impervious surface;  $Y_i$  is the actual fraction of impervious surface; and  $N$  is the number of selected samples [5]. Overall, the higher the value of  $R^2$ , the more reliable the results; and the smaller the values of RMSE and MAE, the more accurate the estimation [31–33].

## 3. Results

### 3.1. Minimum Noise Fraction

Figure 3a–f and Table 2 show that the eigenvalue of MNF components 1 to 6 in 2016 were 44.36, 17.32, 6.53, 3.70, 3.02, and 1.53, respectively, in which the contribution rates were 58.02%, 22.65%, 8.54%, 4.84%, 3.95%, and 2.00%, respectively. All eigenvalues of the MNF components were greater than 1. MNF component 1 had the largest eigenvalue, which demonstrated the highest data dimensionality and the clearest spatial characteristics. MNF component 2 showed the high-albedo and low-albedo endmembers. MNF component 3 indicated the soil and vegetation endmembers.

**Table 2.** The eigenvalues and contribution rates of MNF components.

	MNF 1	MNF 2	MNF 3	MNF 4	MNF 5	MNF 6
Eigenvalue	44.36	17.32	6.53	3.70	3.02	1.53
Contribution rate	58.02%	22.65%	8.54%	4.84%	3.95%	2.00%

### 3.2. Endmember Selection

High-albedo refers to a high reflectance, due to some special-material buildings and different infrastructures, while low-albedo mainly contains residential buildings, shade, and water. Vegetation indicated grass and trees, and soil land comprised bare soil, sand or rock, and construction areas. A water mask is required to be applied in advance to attain more accurate results.

Figure 4a–c shows the selected endmember's scatter plots, in which MNF1-MNF2 is corresponding to high-albedo, low-albedo, and vegetation, while MNF1-MNF3 to vegetation, low-albedo, and soil, and MNF 2-MNF3 to high-albedo, low-albedo, and vegetation [14]. The noise fraction, i.e., heterogeneous spatial-spectral signs, is represented by black dots diffusing at angles of the triangle.

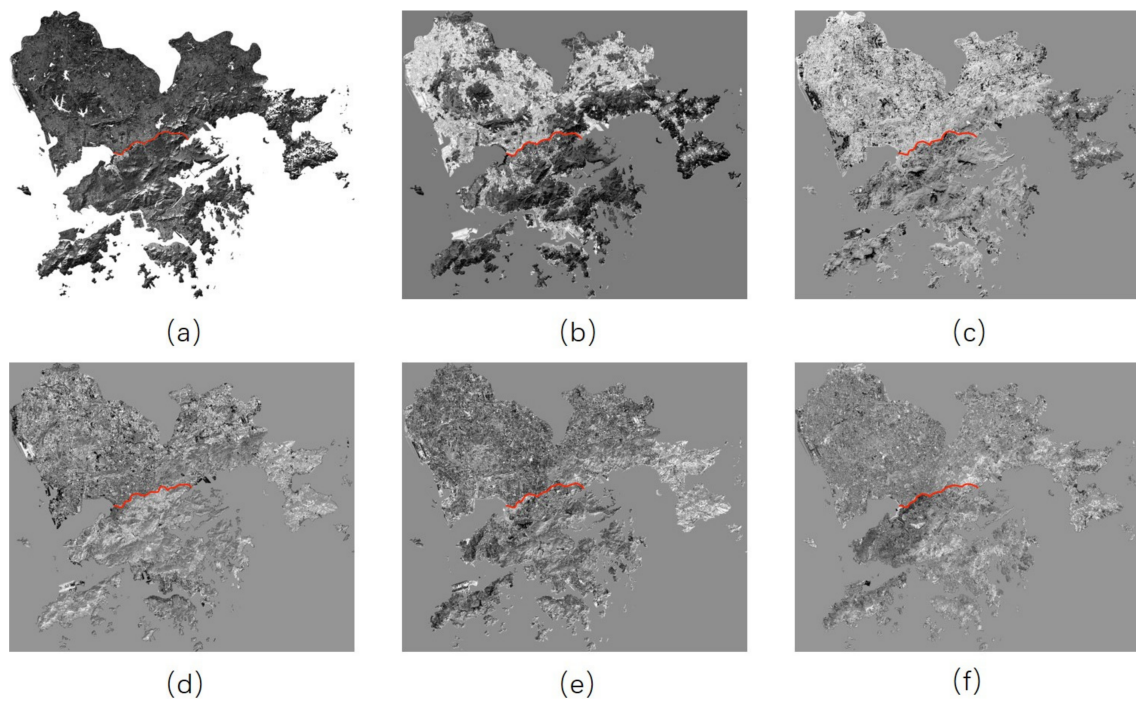


**Figure 3.** MNF components: (a) MNF Component 1; (b) MNF Component 2; (c) MNF Component 3; (d) MNF Component 4; (e) MNF Component 5; (f) MNF Component 6.

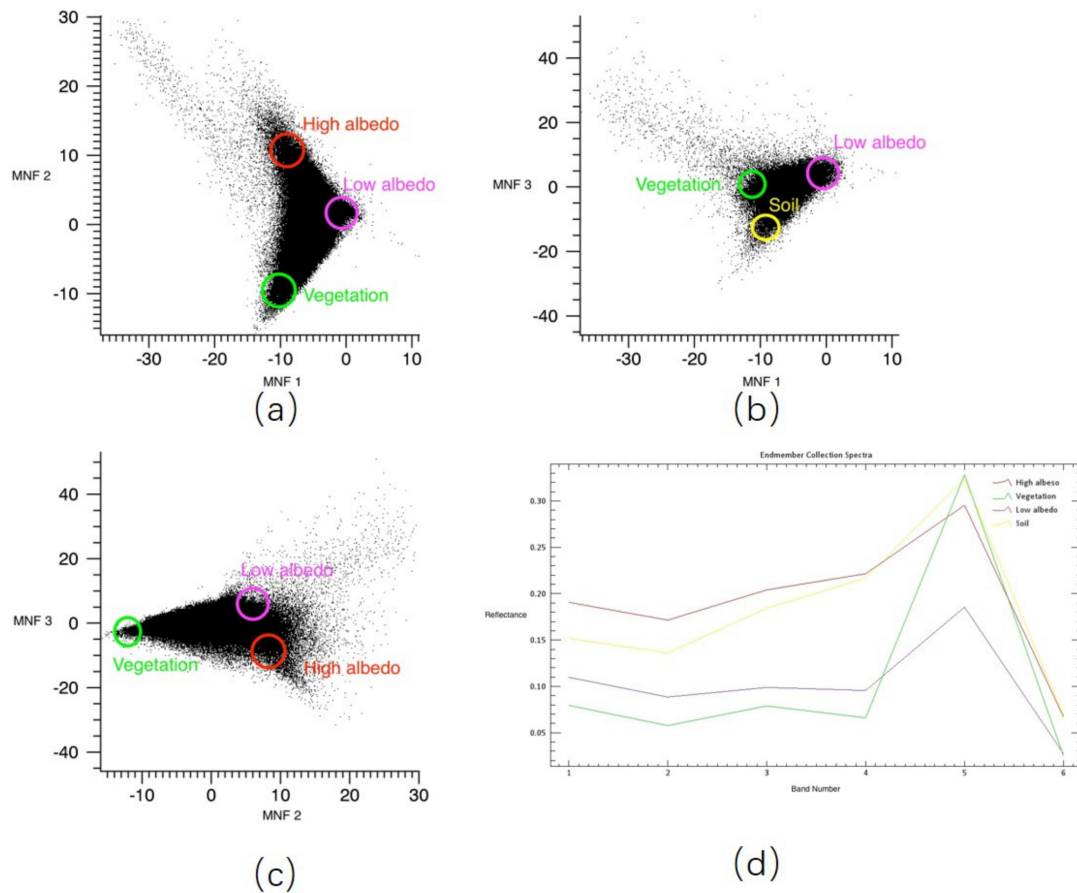


**Figure 4.** Two-dimensional scatter plot of MNF1–MNF2 and the reflectance of the four endmembers: (a) 2D scatter plot of MNF1–MNF2; (b) 2D scatter plot of MNF1–MNF3; (c) 2D scatter plot of MNF2–MNF3; (d) the reflectance of the four endmembers.

Figure 4d shows the reflectance of the four endmembers. From band 1 to 4, high-albedo showed the highest reflectance, soil exhibited the second-highest reflectance, low-albedo showed the third-largest reflectance, and vegetation exhibited the lowest reflectance. In band 5, vegetation exhibited the largest reflectance, soil showed the second-largest reflectance, high-albedo exhibited the third-largest reflectance, and the lowest reflectance was shown by low-albedo. Figure 5 shows an example of the water mask in 2016.

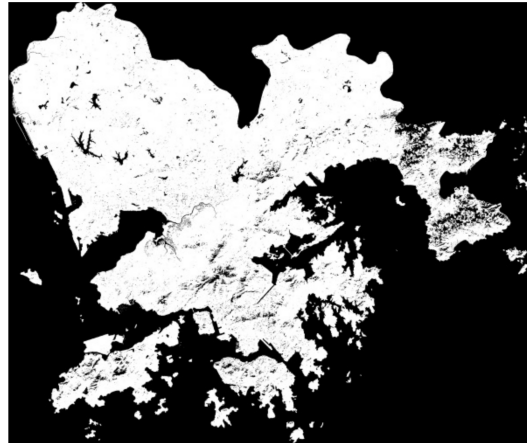


**Figure 5.** An example of the land area of Hong Kong and Shenzhen in 2016 after the water was masked.

### 3.3. Linear Spectral Un-Mixing

Linear spectral un-mixing approach was applied to analyze the following five layers: low-albedo, high-albedo, vegetation, soil, and root mean square error (RMSE) [14,27,34,35]. The bright area indicated the infrastructures for the high-albedo layer, a high density of residential buildings in the urban area for the low-albedo layer, the bare area and rock for the soil layer, and the mountain, grass, and trees for the vegetation reflectance layer.

Table 3 presents the rates obtained with linear spectral un-mixing analysis, which is consistent with and supports the previous results in the same selected study areas in Shenzhen and Hong Kong [13,14]. Regarding Shenzhen and Hong Kong, in 2016, Figure 6a–d presents the examples of the results of the linear spectral un-mixing analysis.

**Table 3.** The proportion of high-albedo, low-albedo, soil, and vegetation of Hong Kong and Shenzhen in 1995, 2005, and 2016.

Study Area	Type/Year	1995	2005	2016
Hong Kong	High-albedo	12.34%	12.63%	12.94%
	Vegetation	47.24%	46.69%	46.27%
	Low-albedo	24.12%	25.18%	25.56%
	Soil	16.30%	15.50%	15.24%
Shenzhen	High-albedo	17.40%	21.47%	25.60%
	Vegetation	34.99%	33.42%	33.94%
	Low-albedo	24.33%	27.57%	37.36%
	Soil	23.28%	17.53%	10.37%

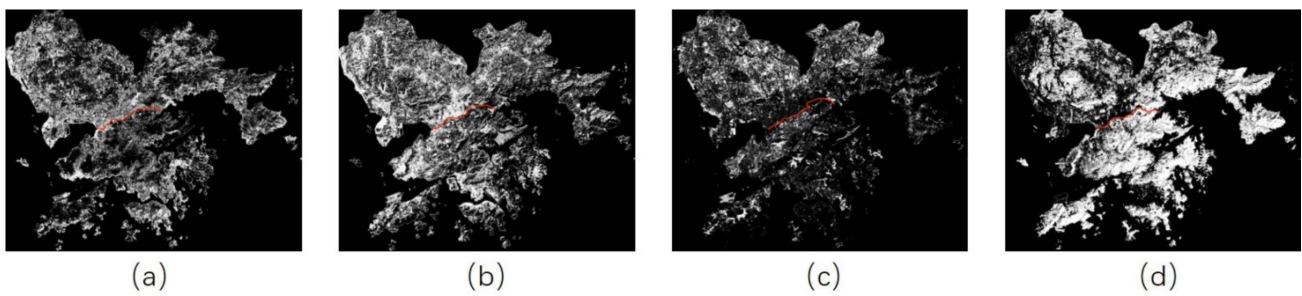


**Figure 6.** Linear spectral un-mixing of Hong Kong and Shenzhen in 2016: (a) high-albedo; (b) low-albedo; (c) soil; (d) vegetation.

### 3.4. Impervious Surface Estimation

Impervious surface estimation was obtained from the combination of high-albedo and low-albedo, in which the brighter the area, the higher the fraction of impervious surface.

Figure 7a–c shows the impervious surface proportions of Hong Kong and Shenzhen in 1995, 2005, and 2016. Over each decade, the impervious surface area of Shenzhen rose markedly, while that of Hong Kong increased only slightly. The impervious surface proportions of Hong Kong in 1995, 2005, and 2016 were 36.64%, 37.80%, and 38.49%, respectively, with the increase rates of 3.68% from 1995 to 2005 and 1.83% from 2005 to 2016, and the average increase rate from 1995 to 2016 was 5.5%. The impervious surface proportions of Shenzhen in 1995, 2005, and 2016 were 15.38%, 19.62%, and 25.23%, respectively, with an increase rate of 27.57% from 1995 to 2005 and 28.59% from 2005 to 2016, and the average increase rate from 1995 to 2016 was 64.04%.

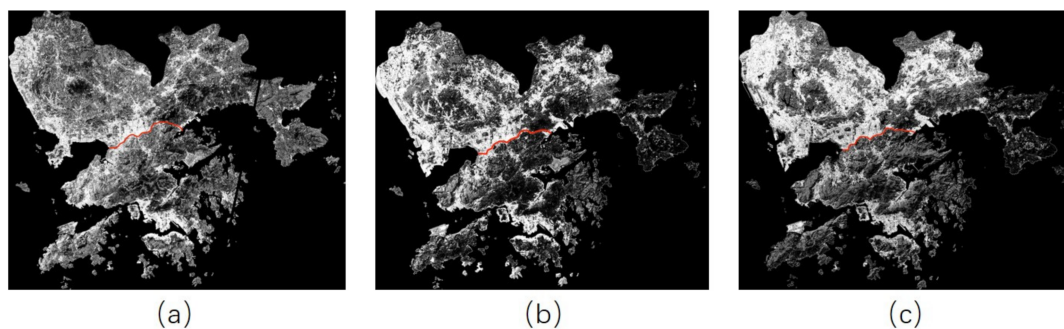


**Figure 7.** Impervious surface fraction of Hong Kong and Shenzhen: (a) 1995; (b) 2005; (c) 2016.

The increase in impervious surfaces in Hong Kong was mainly caused by reclaimed areas, i.e., Pillar Point (Figure 8a) and the Hong Kong Disneyland Resort (Figure 8b) from 1995 to 2005, and the northeastern part of Chek Lap Kok and the seawall of the Hong Kong-Zhuhai-Macau Bridge (Figure 8c) from 2005 to 2016. The increase in impervious surfaces in Shenzhen was due to land creation [36], i.e., the central, eastern, and western part of the Bao'an District (Figure 9a) and the expansion of the Longgang District (Figure 9b) from 1995 to 2005, and the southeastern part of the Nanshan District (Figure 9c) and the southeastern part of the Yantian District (Figure 9d) from 2005 to 2016.

### 3.5. Accuracy Assessment

Figure 10 shows the assessment of accuracy using root mean square error (RMSE) in the fifth layer of the linear spectral un-mixing analysis [14]. The level of acceptance should be less than 0.02. The mean value of the RMSE was 0.0045 in 1995, 0.0035 in 2005, and 0.0013 in 2016. Therefore, a high accuracy level was achieved.

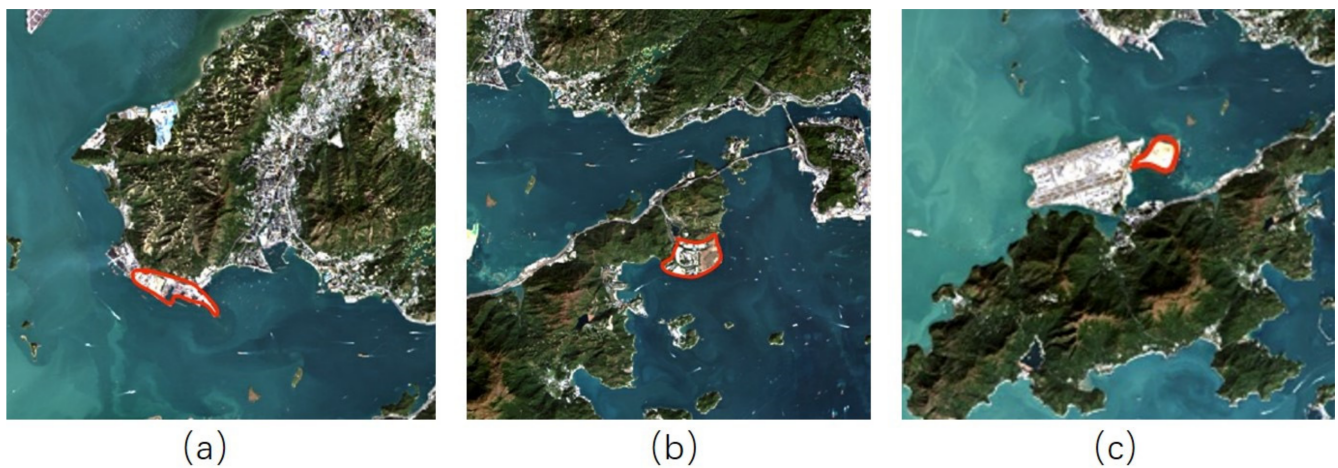


**Figure 8.** The increase in impervious surface areas of Hong Kong: (a) Pillar Point; (b) Hong Kong Disneyland Resort; (c) the Hong Kong-Zhuhai-Macau Bridge.

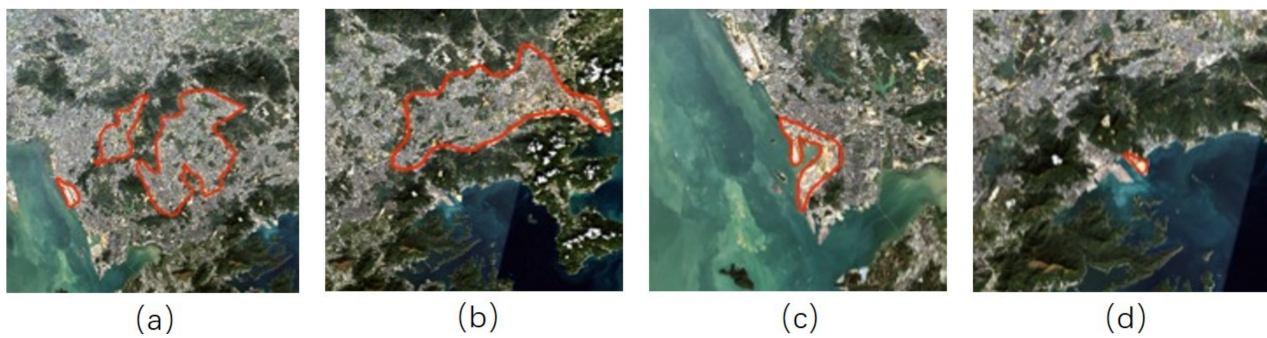


**Figure 9.** The increase in impervious surface areas of Shenzhen: (a) the central, eastern, and western part of the Baoan District; (b) the expansion of the Longgang District; (c) the expansion of the southeastern part of the Nanshan District; (d) the southeastern part of the Yantian District.



**Figure 10.** RMSE (root mean square error) results in 2016.

The RMS value was high in the region of 0–0.0045 in 1995, 0–0.0035 in 2005, and 0–0.0013 in 2016. Normally, Shenzhen was mainly located in between the high-albedo and soil regions, as high-albedo was complex, and soil contained different materials. In comparison, Hong Kong was distributed mainly in between vegetation and low-albedo

regions for the fact that the mountains exerted a shading effect on some vegetation areas that would be classified as low-albedo. Consequently, accuracy might have been influenced, as ascribed to the increased complexity of endmember classification.

To validate the results, SPOT images with a spatial resolution of  $10\text{ m} \times 10\text{ m}$  dimensions and Google Earth images were utilized to assess the accuracy of the results. The real fractions of endmember fractions were digitized through the examples of SPOT images and Google Earth images (Figure 11).

Study Area	Landsat TM Image	SPOT Image	Google Earth Image
Hong Kong (22°17'31" N, 114°09'50" E)			
Hong Kong (22°22'44" N, 114°12'53" E)			
Hong Kong (22°23'39" N, 114°00'49" E)			
Shenzhen (22°35'53" N, 114°127'125" E)			
Shenzhen (22°29'53" N, 114°127'125" E)			
Shenzhen (22°33'04" N, 114°00'56" E)			

**Figure 11.** Random samples of Landsat TM, SPOT, and Google Earth images.

A total of 100 random-sampling,  $3 \times 3$  pixel Landsat TM data were chosen for comparison with the equivalent location of Google Earth images (Figure 12), which shows the residual analysis and calculated RMSE and MAE of impervious surface estimation in 1995, 2005, and 2016.

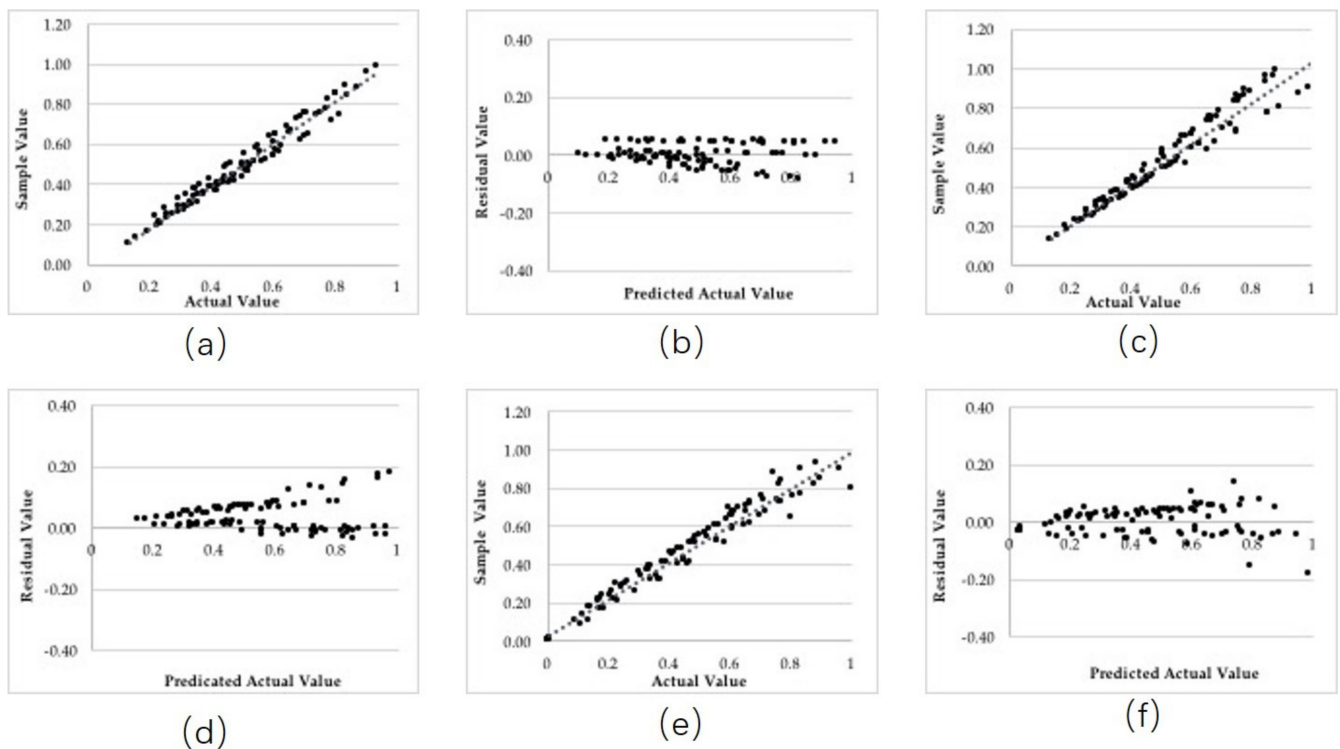


Figure 12. Regression results and residual results: (a,b) 1995; (c,d) 2005; (e,f) 2016.

Figure 12a,c,e shows the results of the regression model for the actual value and predicted value in 1995, 2005, and 2016 [8]. Table 4 shows that the value of  $R^2$  of the Landsat TM images was 0.97 in 1995, 0.95 in 2005, and 0.96 in 2016, which was acceptable. The values of RMSE (Equation (4)) and MAE (Equation (5)) were 3.67% and 2.98% in 1995, 6.36% and 4.49% in 2005, and 4.92% and 4.12% in 2016. The residual analysis is demonstrated in Figure 12b,d,f, and the value range was between 0.2 to  $-0.2$ .

Table 4. The value of  $R^2$  of the Landsat TM image in 1995, 2005, and 2016.

	1995	2005	2016
Value of $R^2$	0.97	0.95	0.96
$n = 100$	RMSE = 3.67%, MAE = 2.98%	RMSE = 6.36%, MAE = 4.49%	RMSE = 4.92%, MAE = 4.12%

Similar to the previous studies [13,14], the highest amount of error of more than 70% in most samples was underestimated when compared with the actual fraction, although some sample fractions of soil and vegetation were overestimated, which should be lower than 0.25 of the abundance rate. The result was affected, since the shade portion of soil and vegetation may have been considered as low-albedo. Relatively high accuracy was reflected from the statistics of  $R^2$ , RMSE, and MAE (see Table 4).

#### 4. Discussion

##### 4.1. Change Related to Land Use and Land Cover

##### 4.1.1. Change in the Fractions of Endmembers and Impervious Surfaces

Hong Kong had an increase of 4.82% in the high-albedo fraction, a decrease of 2.05% in the vegetation fraction, an increase of 5.96% in the low-albedo fraction, and a decrease of 6.51% in soil (Figure 13). Regarding Shenzhen, high-albedo increased by 47.16%, vegetation dropped by 30.16%, low-albedo rose by 53.58%, and soil decreased by 55.47% (Figure 13). The overall increases in the impervious surface fractions of Hong Kong and Shenzhen were

5.58% and 50.90%, respectively (see Figure 14). The expansion in high-albedo, low-albedo, and impervious surfaces in Shenzhen was greater than in Hong Kong from 1995 to 2016.

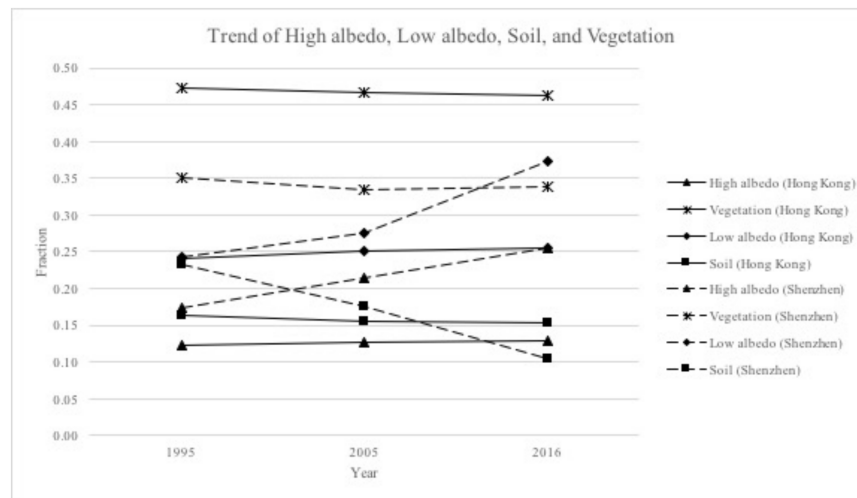


Figure 13. Trend of high-albedo, low-albedo, soil, and vegetation for Hong Kong and Shenzhen.

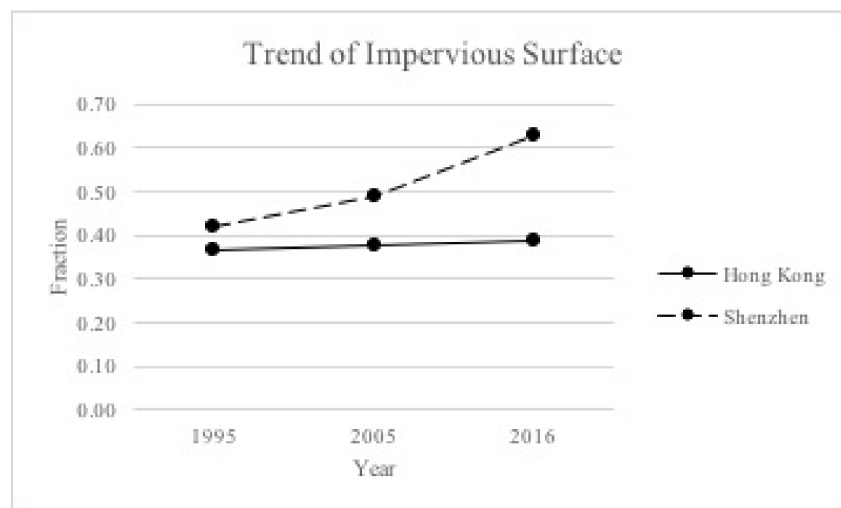


Figure 14. Trend of impervious surface for Hong Kong and Shenzhen.

#### 4.1.2. Change in the Trend of Land, Sea, and Impervious Surface

Figure 15 presents the trends in Shenzhen and Hong Kong for change in the land, sea, and impervious surface. The calculated total areas of Hong Kong and Shenzhen were 2755 km<sup>2</sup> and 3140 km<sup>2</sup>, respectively, which comprised areas of land and sea. Table 5 shows the percentages and areas of land, sea, and the impervious surface of Hong Kong and Shenzhen. Regarding Hong Kong, from 1995 to 2016, land area rose 12.04%, sea area decreased 4.74%, and impervious surface increased 5.57%. Shenzhen had an 8.37% growth in land area, a 10.92% decline in sea area, and a 50.91% growth in impervious surface area from 1995 to 2016. Hong Kong and Shenzhen have distinctly different land policies and thus, Hong Kong had a slight increase in urban areas and Shenzhen had a dramatic increase in urban areas from 1995 to 2016 (Table 5).

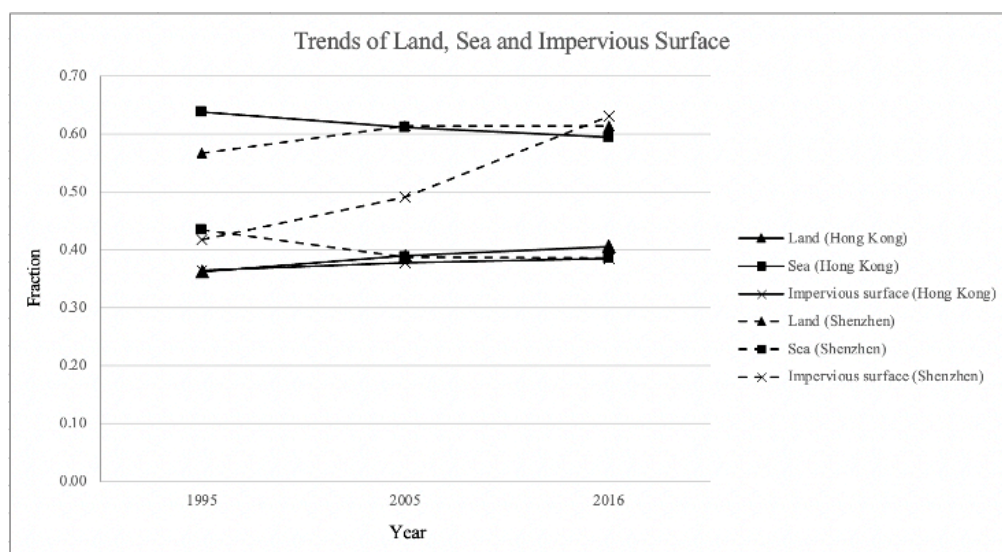


Figure 15. Trends of land, sea, and impervious surface.

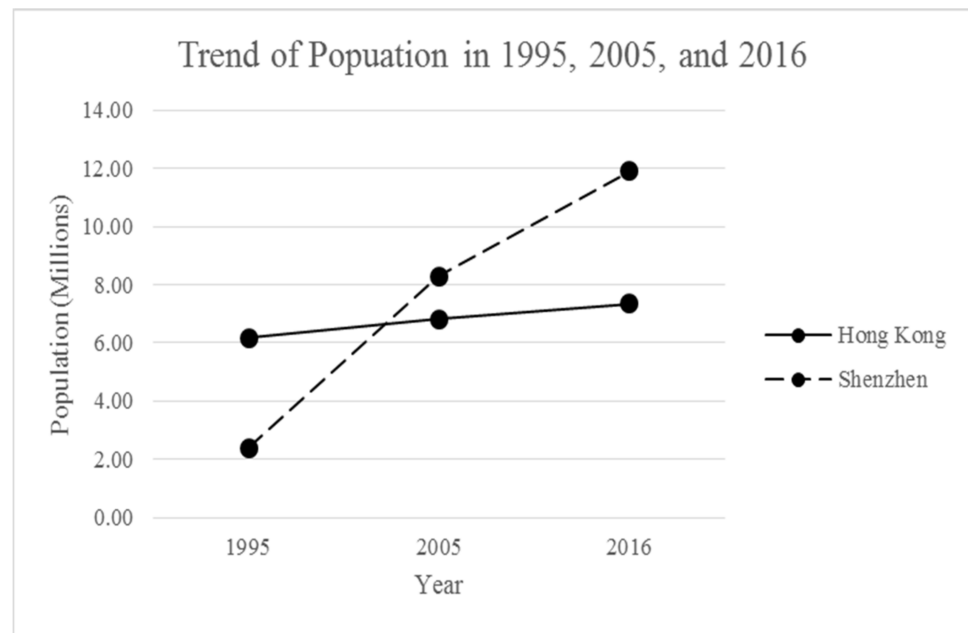
Table 5. Percentage and area of land, sea, and impervious surface of Hong Kong and Shenzhen.

Study Area	Type/Year	1995	2005	2016
Hong Kong	Land	36.21% 997.59 km <sup>2</sup>	38.94% 1072.80 km <sup>2</sup>	40.57% 1117.70 km <sup>2</sup>
	Sea	63.79% 1757.41 km <sup>2</sup>	61.06% 1682.20 km <sup>2</sup>	59.43% 1637.30 km <sup>2</sup>
	Impervious surface	36.46% 362.72 km <sup>2</sup>	37.80% 405.51 km <sup>2</sup>	38.49% 430.20 km <sup>2</sup>
Shenzhen	Land	56.61% 1777.55 km <sup>2</sup>	61.28% 1924.19 km <sup>2</sup>	61.35% 1926.39 km <sup>2</sup>
	Sea	43.39% 1362.44 km <sup>2</sup>	38.72% 1215.80 km <sup>2</sup>	38.65% 1213.61 km <sup>2</sup>
	Impervious surface	41.72% 741.59 km <sup>2</sup>	49.04% 943.62 km <sup>2</sup>	62.96% 1212.85 km <sup>2</sup>

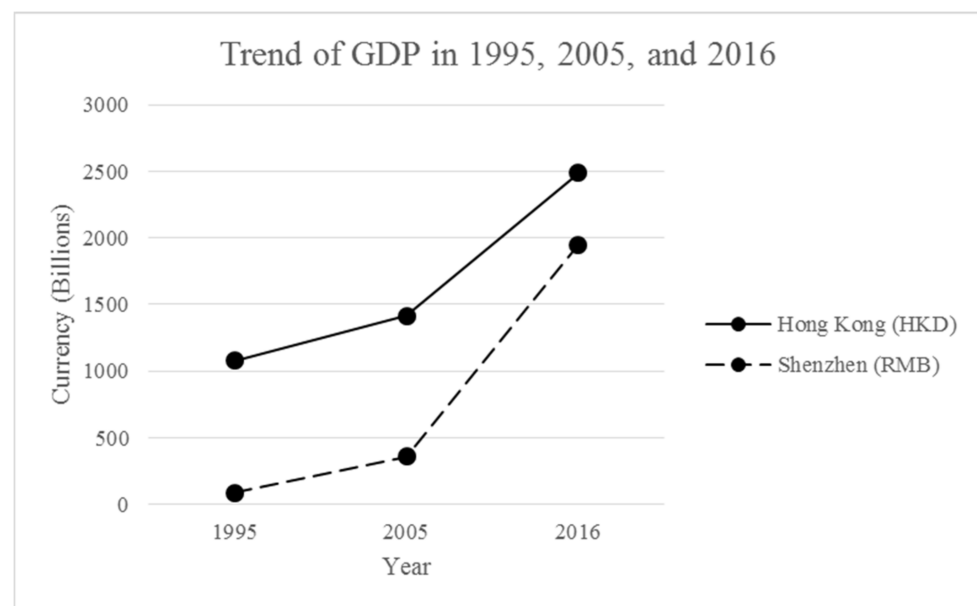
4.2. The Relationship between Impervious Surfaces, Gross Domestic Product, and Population

Figure 16 illustrates the population trend of Hong Kong and Shenzhen in 1995, 2005, and 2016. The population of Hong Kong constitutes an increase rate of 10.55% from 1995 to 2005 and 7.78% from 2005 to 2016. The overall rate of Hong Kong’s population growth from 1995 to 2016 was 19.16% [37–39]. The population of Shenzhen exhibited an increase rate of 246.44% from 1995 to 2005 and 43.84% from 2005 to 2016, and the overall population rate increase was 398.33% [40–42].

The GDP trend of Hong Kong and Shenzhen in 1995, 2005, and 2016 is presented in Figure 17. The GDP of Hong Kong exhibited an increase rate of 31.10% from 1995 to 2005 and 76.27% from 2005 to 2016, and the overall GDP rate increase was 131.10%. The GDP of Shenzhen exhibited an increase rate of 327.38% from 1995 to 2005 and 443.18% from 2005 to 2016, and the overall increase rate was 2221.43%.



**Figure 16.** Trend of population in 1995, 2005, and 2016.



**Figure 17.** Trend of GDP in 1995, 2005, and 2016.

Figure 18 shows the trend of GDP per capita of Hong Kong and Shenzhen in 1995, 2005, and 2016. The GDP per capita of Hong Kong exhibited an increase rate of 18.59% from 1995 to 2005 and 63.55% from 2005 to 2016, and the overall increase rate was 93.95%. The GDP per capita of Shenzhen exhibited an increase rate of 23.36% from 1995 to 2005 and 277.60% from 2005 to 2016, and the overall increase rate was 365.80%. Table 6 summarizes the population, GDP, GDP per capita of Hong Kong and Shenzhen in 1995, 2005, 2016.

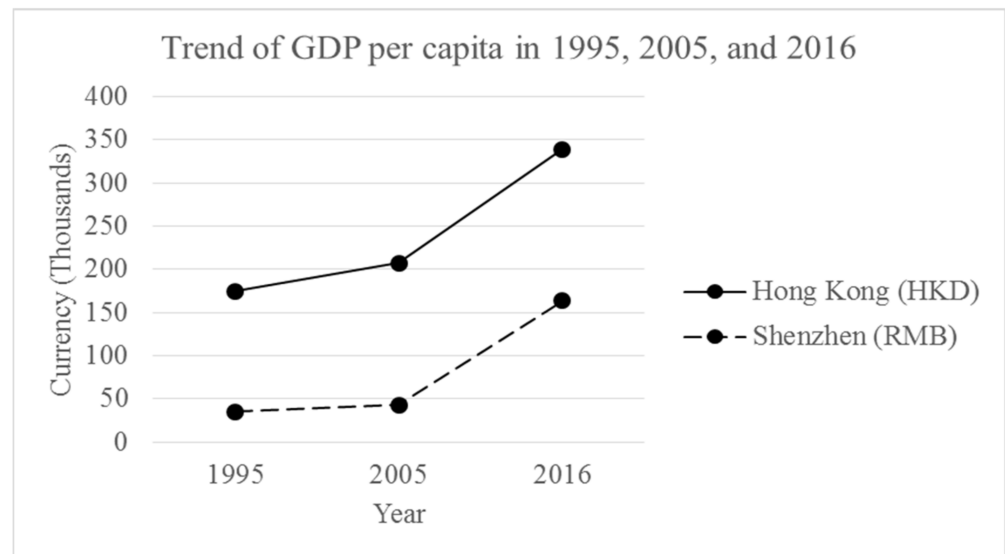


**Figure 18.** Trend of GDP per capita in 1995, 2005, and 2016.

**Table 6.** Population, GDP, GDP per capita of Hong Kong and Shenzhen in 1995, 2005, and 2016.

Type/Year		1995	2005	2016
Hong Kong	Population (Million)	6.15	6.78	7.31
	GDP (Billion HKD)	761	1291	2397
	GDP per capita (Thousand HKD)	123.73	190.41	327.91
Shenzhen	Population (Million)	2.39	5.98	10.75
	GDP (Billion RMB)	79	342	1750
	GDP per capita (Thousand RMB)	33.05	57.19	162.79

Hong Kong exhibited a steady increase in population from 1995 to 2016, and Shenzhen had a sharp increase in population growth from 1995 to 2016. The GDP and GDP per capita of Hong Kong and Shenzhen from 1995 to 2005 increased steadily, and from 2005 to 2016 they increased sharply. The growth of population, GDP, GDP per capita, and the two study areas showed a positive correlation. The increase in population growth in Hong Kong, as well as GDP, was probably due to the strong economic development in the free market, taxation, and service industries [43,44]. The increase in population and GDP in Shenzhen was probably attributable to reform and opening contributing to the rapid development of financial industries and information technologies industries [45]. To cope with the increasing population, more areas in Hong Kong and Shenzhen were developed into urban areas. However, the increase in impervious surface area in Hong Kong was relatively smaller than that in Shenzhen, which was ascribed to an entirely different land-use development strategy. In Hong Kong, protection of the ecological environment constituted the core value of the land-use development [46], and thus, reclamation was the main strategy to develop more available land and solidify the coastline against erosion. On the other hand, the land-use development strategy of Shenzhen was land creation [36], which removed soil and mud on the hillsides to create flat land that could be developed into urban areas.

The land-use policies in Hong Kong and Shenzhen possess some unique aspects. For example, Hong Kong's government protects high ecological land areas, resulting in land limitations. Consequently, they employ the strategy of building high-rise buildings to catch up with the rapid population growth. However, the highly dense buildings of the city result in an urban heat island effect [47], which leads to health problems. On the other hand, the land-use policy of Shenzhen's government is characterized by the destruction of biodiverse living areas [48]. Moreover, the conversion of land use results in increasing amounts of greenhouse gases. Although Shenzhen's land-use policy could meet the needs of the population, the ecological environment and biodiversity are at risk.

Many trees and shrubs have been planted in residential areas, as well as on the rooftops of some commercial buildings and residential buildings. These areas may be impervious surfaces; however, they could be mistakenly estimated as vegetation. The mistaken classification between low-albedo and vegetation might influence the amount of impervious surface area. Due to the hilly characteristic of Hong Kong, the enormous mountains generated shade over their surrounding areas, which were classified as low-albedo areas, which affects the estimation of the impervious surface fraction. Moreover, different sea levels at different times affected the total land area being recorded by remote sensors.

#### *4.3. Limitations and Future Research*

This study is not without limitations. The discrepancy between actual areas and estimated areas of four types of land cover is possibly due to the low spatial resolution of the extracted Landsat images, ebb and flood tide affecting the water level, or the environmental green in residential areas. Since Landsat satellite images were taken in different periods of time in 1995, 2005, and 2016, the water level at different periods, e.g., morning tides and evening tides, changes the areas of land cover. Skyrise greenery, including green roofs and vertical greening, is the trend of urban design in Hong Kong, and thus, some urban areas may be classified as vegetation. Regarding future research, classifying land cover based on the V-H-L-S model classification can be developed as a framework for sustainable development analysis. The accuracy of the land-cover classification method used in this study can be assessed in future studies. Furthermore, researchers can compare the accuracy of using the V-I-S model and V-H-L-S model in classifying the land cover to identify which approach is better. High spatial resolution Landsat images, such as SPOT or other advanced satellite imagery, are recommended for application in future studies to improve the classification of land use and land cover and prevent the erroneous classification due to shade. The socio-economic factors in this study include land policies, population growth, GDP, and GDP per capita. The relationship between other socio-economic factors, for instance, lifestyle, purchasing power and educational level, and urban areas expansion can be explored in a future study.

#### **5. Conclusions**

Landsat satellite images can be applied to estimate impervious surface changes in two systems' big cities of one country, such as Hong Kong and Shenzhen. The land areas and impervious surfaces of Hong Kong and Shenzhen increased between 1995 and 2016, which exhibited an inverse proportional relationship with sea area, indicating land reclamation. However, reclamation in Shenzhen was very small from 2005 to 2016 compared to Hong Kong. In addition, the increase in impervious surface areas had a positive correlation with population, GDP, and GDP per capita. Urbanization was probably due to the increase in the population rate and optimistic economic development. However, the increase in urban area development would be governed by land-use development policies. Reclamation for the increase in land use constitutes a primary strategy in Hong Kong due to the promotion of ecological protection. Conversely, land creation in Shenzhen transformed the mountains or other types of land use to flat land for the development of urban areas. Because of the completely different land-use policies and restrictions, Hong Kong only exhibited a slight increase in impervious surface area, while Shenzhen showed a relatively greater increase in

impervious surface area. The challenge for Hong Kong is that a much denser city resulted in an urban heat island, and the challenge for Shenzhen is that land with ecological values was eradicated by urbanization.

While Shenzhen experienced a tremendous increase in the urban area, Hong Kong had a small increase in urban areas under urbanization. This phenomenon demonstrated the concept of “one country, two systems”, which resulted in a radical discrepancy in urban spatial development and distribution of impervious surfaces between the two cities. This difference in the distribution of impervious surfaces in Hong Kong and Shenzhen also reflects the discrepancy of land policies.

**Author Contributions:** Conceptualization, K.W. and Y.Z.; methodology, K.W.; software, K.W.; validation, K.W. and Y.Z.; formal analysis, K.W.; investigation, K.W., Q.C. and M.C.C.; resources, K.W., Y.Z. and J.Y.T.; data curation, K.W.; writing—original draft preparation, K.W.; writing—review and editing, K.W., Y.Z., Q.C. and M.C.C.; visualization, K.W.; supervision, Y.Z. and J.Y.T.; project administration, Y.Z. and J.Y.T.; funding acquisition, K.W. and Y.Z. All authors have read and agreed to the published version of the manuscript.

**Funding:** This research was supported by the National Natural Science Foundation of China (Grant No. U1901215), the Marine Special Program of Jiangsu Province in China (JSZRHYKJ202007), the Natural Scientific Foundation of Jiangsu Province (BK20181413), and the State Key Lab Fund for Geological Processes and Mineral Resources (2016).

**Institutional Review Board Statement:** Not applicable.

**Informed Consent Statement:** Not applicable.

**Data Availability Statement:** Not applicable.

**Acknowledgments:** The data from the website of USGS, MDA and from the Shenzhen and Hong Kong local governments are highly appreciated. This study was supported by the National Natural Science Foundation of China (Grant No. U1901215), the Marine Special Program of Jiangsu Province in China (JSZRHYKJ202007), the Natural Scientific Foundation of Jiangsu Province (BK20181413), and the State Key Lab Fund for Geological Processes and Mineral Resources (2016). Authors also thank the three reviewers’ critical comments to improve the manuscript.

**Conflicts of Interest:** The authors declare no conflict of interest.

## References

1. Shahtahmassebi, A.; Pan, Y.; Lin, L.; Shortridge, A.; Wang, K.; Wu, J.X.; Wu, D.; Zhang, J. Implications of land use policy on impervious surface cover change in Cixi County, Zhejiang Province, China. *Cities* **2014**, *39*, 21–36. [\[CrossRef\]](#)
2. Li, L.; Lu, D.; Kuang, W. Examining Urban Impervious Surface Distribution and Its Dynamic Change in Hangzhou Metropolis. *Remote Sens.* **2016**, *8*, 265. [\[CrossRef\]](#)
3. Bauer, M.E.; Heinert, N.J.; Doyle, J.K.; Yuan, F. Impervious surface mapping and change monitoring using Landsat remote sensing. In Proceedings of the ASPRS annual conference proceedings, Denver, CO, USA, 23–28 May 2004.
4. Espey, W.H.J.; Morgan, C.W.; Masch, F.D. *A Study of some Effects of Urbanization on Storm Runoff from a Small Watershed*; Report 23; Texas Water Development Board: Austin, TX, USA, 1966.
5. Wu, C. Normalized spectral mixture analysis for monitoring urban composition using ETM+ imagery. *Remote Sens. Environ.* **2004**, *93*, 480–492. [\[CrossRef\]](#)
6. Wu, C.; Murray, A.T. Estimating impervious surface distribution by spectral mixture analysis. *Remote Sens. Environ.* **2003**, *84*, 493–505. [\[CrossRef\]](#)
7. Ridd, M.K. Exploring a V-I-S (vegetation-impervious surface-soil) model for urban ecosystem analysis through remote sensing: Comparative anatomy for cities†. *Int. J. Remote Sens.* **1995**, *16*, 2165–2185. [\[CrossRef\]](#)
8. Ji, M.; Jensen, J.R. Effectiveness of subpixel analysis in detecting and quantifying urban imperviousness from Landsat Thematic Mapper imagery. *Geocarto Int.* **1999**, *14*, 33–41. [\[CrossRef\]](#)
9. Wang, W.; Yao, X.; Zhai, J.; Ji, M. A Tetrahedron-Based Endmember Selection Approach for Urban Impervious Surface Mapping. *PLoS ONE* **2014**, *9*, e93479. [\[CrossRef\]](#)
10. Hendrix, E.M.; Garcia, I.; Plaza, J.; Plaza, A. Minimum volume simplicial enclosure for spectral unmixing of remotely sensed hyperspectral data. In Proceedings of the 2010 IEEE International Geoscience and Remote Sensing Symposium, Honolulu, HI, USA, 25–30 July 2010; pp. 193–196. [\[CrossRef\]](#)
11. Liao, W.; Deng, Y.; Li, M.; Sun, M.; Yang, J.; Xu, J. Extraction and Analysis of Finer Impervious Surface Classes in Urban Area. *Remote Sens.* **2021**, *13*, 459. [\[CrossRef\]](#)

12. Shih, H.-C.; Stow, D.A.; Tsai, Y.-M.; Roberts, D.A. Estimating the starting time and identifying the type of urbanization based on dense time series of landsat-derived Vegetation-Impervious-Soil (V-I-S) maps—A case study of North Taiwan from 1990 to 2015. *Int. J. Appl. Earth Obs. Geoinf.* **2020**, *85*, 101987. [CrossRef]
13. Zhang, Y.; Zhang, H.; Lin, H. Improving the impervious surface estimation with combined use of optical and SAR remote sensing images. *Remote Sens. Environ.* **2014**, *141*, 155–167. [CrossRef]
14. Wong, K.P.; Zhang, Y.; Tsou, J.Y.; Li, Y. Assessing Impervious Surface Changes in Sustainable Coastal Land Use: A Case Study in Hong Kong. *Sustainability* **2017**, *9*, 1029. [CrossRef]
15. Fu, B.; Peng, Y.; Zhao, J.; Wu, C.; Liu, Q.; Xiao, K.; Qian, G. Driving forces of impervious surface in a world metropolitan area, Shanghai: Threshold and scale effect. *Environ. Monit. Assess.* **2019**, *191*, 771. [CrossRef] [PubMed]
16. Omurakunova, G.; Bao, A.; Xu, W.; Duulatov, E.; Jiang, L.; Cai, P.; Abdullaev, F.; Nzabarinda, V.; Durdiev, K.; Baiseitova, M. Expansion of Impervious Surfaces and Their Driving Forces in Highly Urbanized Cities in Kyrgyzstan. *Int. J. Environ. Res. Public Heal.* **2020**, *17*, 362. [CrossRef]
17. Census and Statistics Department. Hong Kong Population Projections 2015–2064. 2015. Available online: <https://www.statistics.gov.hk/pub/B1120015062015XXXXB0100.pdf> (accessed on 6 April 2016).
18. Goodstadt, L.F. *The Global Crisis: Why Laisser-Faire Hong Kong Prefers Regulation* (29 January 2010); HKIMR Working Paper No. 01/2010; SSRN: Rochester, NY, USA, 2010.
19. China Institute of City Competitiveness. Yearbook of China City Competitive 2012. Available online: [http://www.china-citynet.com/yjh/en/zgcsjzlnj\\_show.asp?id=13](http://www.china-citynet.com/yjh/en/zgcsjzlnj_show.asp?id=13) (accessed on 6 April 2016).
20. The Statistics Portal. China: Population of Shenzhen from 1995 to 2030. 2016. Available online: <https://www.statista.com/statistics/466986/china-population-of-shenzhen/> (accessed on 6 April 2016).
21. Lu, D.; Weng, Q. Use of impervious surface in urban land-use classification. *Remote Sens. Environ.* **2006**, *102*, 146–160. [CrossRef]
22. Santamouris, M.; Synnefa, A.; Karlessi, T. Using advanced cool materials in the urban built environment to mitigate heat islands and improve thermal comfort conditions. *Sol. Energy* **2011**, *85*, 3085–3102. [CrossRef]
23. Adam, J.B.; Smith, M.O.; Johnson, P.E. Spectral mixture modeling: A new analysis of rock and soil types at the Viking Landsat site. *J. Geogr. Res.* **1986**, *91*, 8098–8112. [CrossRef]
24. Rashed, T.; Weeks, J.R.; Roberts, D.; Rogan, J.; Powell, R. Measuring the Physical Composition of Urban Morphology Using Multiple Endmember Spectral Mixture Models. *Photogramm. Eng. Remote Sens.* **2003**, *69*, 1011–1020. [CrossRef]
25. Weng, Q.; Hu, X.; Lu, D. Extracting impervious surfaces from medium spatial resolution multispectral and hyperspectral imagery: A comparison. *Int. J. Remote Sens.* **2008**, *29*, 3209–3232. [CrossRef]
26. Weng, Q.; Hu, X.; Liu, H. Estimating impervious surface using linear spectral mixture analysis with multi-temporal ASTER image. *Int. J. Remote Sens.* **2009**, *30*, 4807–4830. [CrossRef]
27. Small, C. Estimation of urban vegetation abundance by spectral mixture analysis. *Int. J. Remote Sens.* **2001**, *22*, 1305–1334. [CrossRef]
28. Welch, R. Spatial resolution requirements for urban studies. *Int. J. Remote Sens.* **1982**, *3*, 139–146. [CrossRef]
29. Madhavan, B.B.; Kubo, S.; Kurisaki, N.; Sivakumar, T.V.L.N. Appraising the anatomy and spatial growth of the Bangkok Metropolitan area using a vegetation-impervious-soil model through remote sensing. *Int. J. Remote Sens.* **2001**, *22*, 789–806. [CrossRef]
30. Setiawan, H.; Mathieu, R.; Thompson-Fawcett, M. Assessing the applicability of the V-I-S model to map urban land use in the developing world. *Comput. Environ. Urban* **2006**, *30*, 503–522. [CrossRef]
31. Congalton, R.G. A review of assessing the accuracy of classifications of remotely sensed data. *Remote Sens. Environ.* **1991**, *37*, 35–46. [CrossRef]
32. Congalton, R.G.; Green, K. *Assessing the Accuracy of Remotely Sensed Data: Principles and Practices*; CRC Press: Boca Raton, FL, USA, 1999.
33. Foody, G.M. Status of land cover classification accuracy assessment. *Remote Sens. Environ.* **2002**, *80*, 185–201. [CrossRef]
34. Lu, D.; Morán, E.; Batistella, M. Linear mixture model applied to Amazonian vegetation classification. *Remote Sens. Environ.* **2003**, *87*, 456–469. [CrossRef]
35. Lu, D.; Batistella, M.; Morán, E.; Mausel, P. Application of spectral mixture analysis to Amazonian land-use and land-cover classification. *Int. J. Remote Sens.* **2004**, *25*, 5345–5358. [CrossRef]
36. Li, P.; Qian, H.; Wu, J. Environment: Accelerate research on land creation. *Nature* **2014**, *510*, 29–31. [CrossRef] [PubMed]
37. HKSAR Census and Statistic Department. *Hong Kong Annual Digest of Statistics 1995*; HKSAR Census and Statistic Department: Hong Kong, China, 1996.
38. HKSAR Census and Statistic Department. *Hong Kong Annual Digest of Statistics 2005*; HKSAR Census and Statistic Department: Hong Kong, China, 2006.
39. HKSAR Census and Statistic Department. *Hong Kong Annual Digest of Statistics 2015*; HKSAR Census and Statistic Department: Hong Kong, China, 2016.
40. Department of Population and Employment Statistics of the National Bureau of Statistics of China. *China Population Statistics Yearbook 1995*; China Statistics Press: Beijing, China, 1995.
41. Department of Population and Employment Statistics of the National Bureau of Statistics of China. *China Population Statistics Yearbook 2005*; China Statistics Press: Beijing, China, 2005.

42. Department of Population and Employment Statistics of the National Bureau of Statistics of China. *China Population Statistics Yearbook 2016*; China Statistics Press: Beijing, China, 2016.
43. Wong, Y.C.R. Hong Kong in Transition Economic Transformation in the Eighties. In Proceedings of the Conference on the Changing World Community: Development Consequences and Adjustments in Asia and the Pacific, Ninth General Meeting, Association of Development Research and Training Institutes of Asia and the Pacific, Macau, China, 8–11 October 1991.
44. Lin, C.W.; Wong, K. Economic Growth and International Trade: The Case of Hong Kong. 1997. Available online: <https://faculty.washington.edu/karyiu/papers/Gro&Tra-HKP.pdf> (accessed on 6 April 2016).
45. Ng, M.K.; Tang, W.-S. The Role of Planning in the Development of Shenzhen, China: Rhetoric and Realities. *Eurasian Geogr. Econ.* **2004**, *45*, 190–211. [[CrossRef](#)]
46. Xie, H.L.; He, Y.F.; Xie, X. Exploring the factors influencing ecological land change for China's Beijing–Tianjin–Hebei Region using big data. *J. Clean. Prod.* **2017**, *142*, 677–687. [[CrossRef](#)]
47. An, X.; Ng, E.; Ren, C. Urban Heat island in Hong Kong. Department of Architecture. The Chinese University of Hong Kong. 2006. Available online: <http://geography.ccsc.edu.hk/al/urbanheatislandHK.pdf> (accessed on 6 April 2016).
48. Peng, Y.; Qian, J.; Ren, F.; Zhang, W.; Du, Q. Sustainability of land use promoted by Construction-to-Ecological Land Con-version: A Case Study of Shenzhen City, China. *Sustainability* **2016**, *8*, 671. [[CrossRef](#)]